Proc. Natl. Acad. Sci. USA
Vol. 82, pp. 1131–1135, February 1985
Cell Biology

Monte Carlo study of the GTP cap in a five-start helix model of a microtubule

(phase changes/macroscopic rate constants/attached microtubules/comparison with experiment)

YI-DER CHEN AND TERRELL L. HILL

Laboratory of Molecular Biology, National Institute of Arthritis, Diabetes and Digestive and Kidney Diseases, National Institutes of Health, Bethesda, MD 20205

Contributed by Terrell L. Hill, October 10, 1984

ABSTRACT **Earlier Monte Carlo studies on a single-helix model of the GTP cap at the end of a microtubule are extended here to a more realistic five-start helix model of the microtubule end. As in the earlier work, phase changes occur at the microtubule end: the end is either capped with GTP and growing slowly or uncapped and shortening rapidly, and these two regimes alternate (at a given tubulin concentration) at steady state. Macroscopic rate constants for the two-phase model are deduced from the Monte Carlo results. The macroscopic rate constants lead to properties that are in semiquantitative agreement with related experiments of Mitchison and Kirschner.**

In an earlier paper (1), we studied phase changes at the end of a microtubule (MT) with a GTP cap by using a single-helix model and the Monte Carlo method. The two phases correspond to the presence (phase 1) of a GTP cap at the MT end or to the absence (phase 2) of such a cap. A MT in phase 1 lengthens slowly; in phase 2 it shortens rapidly. These phase changes are consistent with the experimental work of Carlier *et al.* (2) and of Mitchison and Kirschner (3, 4). The rate constants used in the above-mentioned Monte Carlo kinetic model (1) arose from the fitting of the dilution experiments described in ref. 2.

Although the Monte Carlo treatment of the single-helix kinetic model correctly produced the phase changes that were anticipated from the experiments (3, 4), the question naturally arises as to whether this theoretical result might be a property of the single-helix model itself rather than of a MT. This model is, in fact, appropriate for actin but it represents a considerable approximation when used for a MT: it assumes that the multihelices in a MT (e.g., five, if we assume growth via a five-start helix) are kinetically independent of each other.

In the present paper, we extend the Monte Carlo work to a five-start helix model for the growth of a MT. There are several plausible sets of rules governing MT growth that might be adopted. Because of the complexity of the computer programming, we select what seems to us to be the simplest explicit model. This model produced the desired phase changes without difficulty. Details are given below. These results serve essentially as an "existence theorem": more complicated models of MT growth and somewhat different microscopic kinetics than that used below might prove, in the future, to be more realistic but the present model shows at least that multihelix kinetic models, as well as single-helix models, can generate phase changes (cap, no cap) at the end of a MT. The experimental work of Carlier *et al.* (2) and of Mitchison and Kirschner (3, 4) seems to impose the requirement of phase changes on any detailed model of a MT end.

In choosing parameters in the present work, we have been guided by the experiments of Mitchison and Kirschner (3, 4) rather than by those of Carlier *et al.* (2). We have not attempted optimal fitting of these experiments because of the considerable expense of the calculations. But we found it easy to achieve semiquantitative agreement with some of the main results of Mitchison and Kirschner.

The model

The (flattened) five-start helical structure we assume (5) is shown in Fig. 1*a*. That is, growth (or shortening) of the vertical 13-strand helix occurs only by gain (or loss) of individual subunits at the exposed tips ($n = 1$) of the five helices I, ..., V. Further, we assume that no subunit vacancies or "overhangs" occur. For example, for the particular structure in Fig. 1*a*, a subunit cannot be added to helix III nor can a subunit be lost from helix IV, for both of these events would create an overhang. With these assumptions, each added subunit at any allowed position creates two new nearest-neighbor interactions and each departing subunit gives up two nearest-neighbor interactions. The physical structure of the MT end in Fig. 1*a* is designated 3,6,0,3,1 (the exposed top surface of helix II contains three subunits, the top surface of III contains six subunits, etc.). These five integers must add to 13.

Following earlier work (6), Fig. 2*a* summarizes the microscopic transitions that are possible for each of the five helices (unless an overhang is created; in this case the transition is not allowed). The symbol T refers to a subunit (tubulin dimer) with GTP bound; D refers to a subunit with GDP bound. The T $\rightarrow$ D reactions (κ' and κ) represent the hydrolysis of GTP; the $n = 1$ D $\rightarrow$ T reaction (κ'') is the exchange of GTP for GDP on the helix tip; and the α_2 reaction is the loss of a subunit with GDP bound followed by rapid exchange of GTP for GDP on the subunit in solution. The concentration of T in solution is c. The attachment transition ($\alpha_1 c$) in Fig. 2*a* is actually subdivided, as in Fig. 2*b*, depending on whether the T from solution attaches to a T or to a D at $n = 1$. It is known that $\alpha_{1T} >> \alpha_{1D}$ (7). The computer program also includes an analogous subdivision of α_2 and α_{-1} (6) but this feature is not used in the present paper.

Nearest neighbors in the two-dimensional lattice of Fig. 1*a* are also assumed to influence the interior ($n \geq 2$) hydrolysis rate constant κ. Along a helix (Fig. 1*b*), a T at any position $n \geq 2$ has four possible sets of neighbors at $n - 1$, $n + 1$: DD, DT, TD, and TT. A multiplicative dimensionless factor h_{ij} (i, j = D, T) is introduced to allow for different effects of these neighbors on κ, essentially as in refs. 1 and 2. In the other lattice direction (vertically in Fig. 1*a*), nearest neighbors in other helices may also influence the κ for any T, as indicated schematically in Fig. 1*c*. In the downward direction (Fig. 1*a* and *c*), the two neighbors might be 0D, 0T, DD, DT, TD, and TT. The zero indicates a missing neighbor, as, for example, would be the case for a T at position $n = 4$ of helix III in Fig.

The publication costs of this article were defrayed in part by page charge payment. This article must therefore be hereby marked "*advertisement*" in accordance with 18 U.S.C. §1734 solely to indicate this fact.

Abbreviation: MT, microtubule.

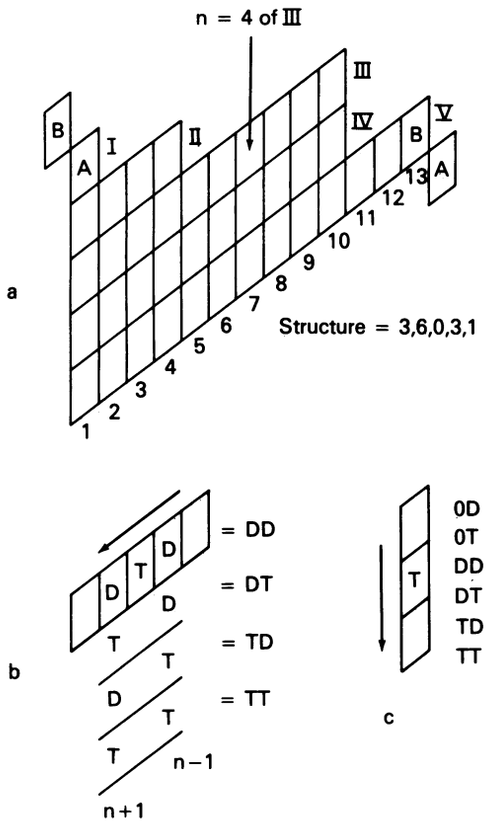

FIG. 1. (*a*) Schematic picture of the arrangement of subunits at the end of a 13-strand MT, growing via a five-start helix model. The helices are labeled I, ..., V. The tip subunit in each helix is designated $n = 1$, the next is $n = 2$, etc. The subunits marked A and B are shown twice. No vacancies or overhangs are allowed, by assumption. The particular surface structure shown here is labeled 3,6,0,3,1. (*b*) Four possible nearest-neighbor pairs of a given T at n, along a given helix, at positions $n - 1$, $n + 1$. (*c*) Six possible nearest-neighbor pairs of a given T, from neighboring helices, counting downward in ρ. A zero represents a vacancy (above the MT structure).

1*a*. The six dimensionless multiplicative factors here are designated v_{kl}. Thus, an arbitrary T at $n \geq 2$ in any helix has a hydrolysis rate constant $\kappa h_{ij} v_{kl}$, depending on the nearest neighbors of T. Clearly, the computer program must keep track of the structure of the MT end (Fig. 1*a*), of the location of each T at $n \geq 2$ in each helix, and of the states of the four neighbors (including missing neighbors) of each such T.

A set of six parameters each, analogous to v_{kl} above, was

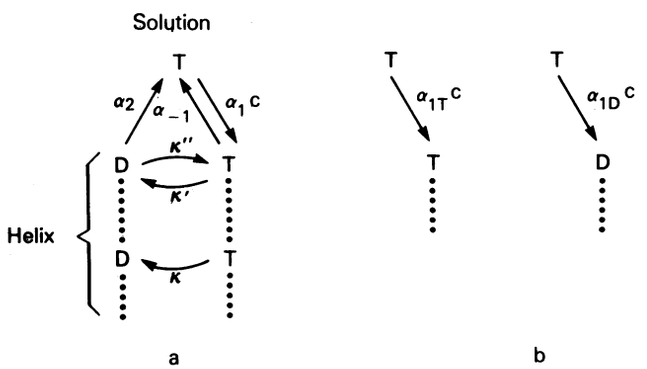

FIG. 2. (*a*) Reactions allowed and first-order rate constants for each helix, unless forbidden by the no-overhang rule. (*b*) Subdivision of α_1 into α_{1T} and α_{1D}, depending on the state at $n = 1$.

also included in the program for possible vertical neighbor influences on κ' and on κ'' (both at $n = 1$). However, these parameters were all set equal to unity (in effect, not used) in the numerical example presented below.

The rate constants in Fig. 2 are all first-order, with units s^{-1}; c has units μM. The rate constants apply to each of the five helices, but possible on and off transitions are reduced somewhat by the no-overhang rule. That is, on the average, somewhat fewer than five helices are available for on-off transitions. The effective number of available helices was reported earlier (5) to be 3.79. A Monte Carlo check in several very simple special cases, using the present program, led to a value of 3.82. The discrepancy was found to be due to a single tallying error (in a structure with degeneracy) in our earlier work (5). The corrected count is as follows: of a total of 476 MT surface or end configurations, 1 has one site (for on or off transitions), 24 have two sites, 132 have three sites, 220 have four sites, and 99 have five sites. The mean number of sites is then 3.8235. A Monte Carlo simulation (at $c = 0$, with a single kind of off transition), using a total of 10^6 transitions, led to 3.8236.

Monte Carlo calculations

These calculations refer to one end of a very long MT at steady state. After a number of trial runs, the set of parameters selected was

$$\kappa = 1.0, \quad \kappa' = 1.0, \quad \kappa'' = 0.10, \quad \alpha_2 = 140,$$
$$\alpha_{1T} = 2.0, \quad \alpha_{1D} = 0.01875, \quad \alpha_{-1} = 0.20. \qquad [1]$$

All of these have units s^{-1} except α_{1T} and α_{1D}, which have units $s^{-1} \cdot \mu M^{-1}$. In addition,

$$h_{DD} = 1.0, \quad h_{DT} = 0.002, \quad h_{TD} = 1.0,$$
$$h_{TT} = 0.002 \qquad [2]$$

$$v_{0D} = 1.0, \quad v_{0T} = 0.5, \quad v_{DD} = 10.0, \quad v_{DT} = 10.0$$
$$v_{TD} = 1.0, \quad v_{TT} = 0.5. \qquad [3]$$

The values in Eq. 2 are the same as in ref. 1. These are designed to keep the Ts in each helix rather compact. Similarly, the choices in Eq. 3 tend to establish similar cap sizes in the different helices. Note that α_{1D} is not zero, as in our previous work. A very small value of α_{1D} (such as this) is not excluded (7).

The procedure followed here is similar to that in refs. 1 and 8. These references should be consulted for general background. We used two simulations of 300,000 transitions each at $c = 0$, 1.5, 3, 4.5, 6, 7, 8, 9, 10, 11, 13, and 15 μM. Each simulation run was preceded by a discard of 10,000 transitions, to ensure a steady state. Time averages of several quantities (e.g., p_1 to p_5, J, J_h) were printed every 200 transitions. Here, p_n is the probability that position n has a T, averaged over the 200 transitions and over all five helices (and normalized to 5.00); J is the mean subunit flux during the 200 transitions, calculated by a generalization (for the overhang rule) of equation 1 of ref. 9; and J_h is the mean GTP hydrolysis rate, calculated by generalizing (overhang rule, h_{ij}, v_{kl}) equations 2 and 3 of ref. 9. The two quite different calculations of J_h provide a self-consistency check.

On the basis of the 200-transition averages, the total time at each c was divided into time spent in phase 1 (growing) or in phase 2 (shortening), and the mean subunit flux was calculated for each category, thus giving J_1 and J_2 (subunit flux in each phase). If f_1 is the fraction of time in phase 1, then

$$f_1/f_2 = k'/k, \quad f_1 + f_2 = 1 \qquad [4]$$

$$J = f_1J_1 + f_2J_2, \quad [5]$$

where k is the rate constant for phase 1 → phase 2, k' is the constant for 2 → 1, and J is the overall mean flux.

The printout for each c gives f_1, from which k'/k follows (Eq. 4). To find k and k' separately, the total number of phase changes in a simulation must be counted. There is a small but not important amount of arbitrariness in deciding what is a phase change and what is not. The mean time per *pair* of phase changes is $(k + k')/kk'$. From this quantity and k'/k, k and k' may be deduced.

Thus, at each c, we have values of J_1, J_2, k, and k'. These are the four rate constants of the relatively simple two-phase macroscopic kinetic model (1, 8) that can be used (as a presumably excellent approximation) in place of the original detailed microscopic kinetic model (Figs. 1 and 2). In this connection, the lifetimes of caps (phase 1) for the cases $c = 7$ through $c = 13$ (156 phase changes, 1 → 2) were examined and were found to be exponentially distributed.

Results for microtubules in solution

Table 1 is a sample from one of the two printouts at $c = 10$. The line labeled 57,200 contains the total time and time averages over transitions 57,001 to 57,200. As can be seen from the p_n and J values, there are two phase changes in the course of this sample (1 → 2 and then 2 → 1). Table 2 presents different information taken from the same simulation (and including the time period of Table 1). This table gives the surface structure (see Fig. 1*a*), the number of Ts in each helix, and the n value of the deepest T in each helix, after 49,000 transitions, after 50,000, etc. These are "snapshots" taken every 1000 transitions. There are three phase changes in the period covered by Table 2, including the two in Table 1. Incidentally, the phase 2 session at 49,000 and 50,000 goes back to 37,000. Table 2 shows typical large fluctuations in the size of the GTP cap and also the wide variety that is observed in the compactness of the cap (compare the last two columns, helix by helix).

Table 3 gives J_h and $\overline{N}$ (number of Ts, in all helices, at $n \geq 2$), averaged over the two simulations at each c, and also the total number of phase changes in the 600,000 transitions at each c. The $\overline{N}$ values refer to the total time (including phase 2 time, during which $\overline{N}$ is very small). At $c = 10$, $\overline{N}$ during phase 1 can be estimated as 232 (about 46 per helix). This is not much larger than the value $\overline{N} = 198$ in the table because the MT end spends most of its time in phase 1.

The values of J_1, J_2, k, and k', at each c, mentioned at the end of the section above, were plotted and smooth curves were drawn through the points. These smooth curves are shown in Figs. 3 (k and k') and 4 (J_1 and J_2). Also included in Fig. 4 are $f_1 = k'/(k + k')$ and J (Eq. 5), calculated from the four smooth curves.

The k and k' curves (Fig. 3) are similar to each other, except that they are reversed in direction. As a consequence, f_1/f_2 (Fig. 4) at the critical concentration ($c_o = 9.97$) is a much reduced 6.40 compared with 103.4 for the same quantity in ref. 1. An estimate of the experimental value (4) for the plus end of the MT is 6.3. Note that $f_1 = 1/2$ where the k and k' curves cross ($c = 7.0$).

The critical concentration, $c_o = 9.97$, agrees with the experimental value (3) (corrected for inactive tubulin). The $J(0)$ value in Fig. 4 is $-374\ s^{-1}$, compared with the experimental value (for the plus end) of $-340\ s^{-1}$ (4). The Monte Carlo J_1 is slightly curved whereas the experimental J_1 is a straight line (4). Also, the Monte Carlo value of J_1 at $c = c_o$ is 13.9 s^{-1} compared with 53 s^{-1} for the plus end (4) (and 16 s^{-1} for the minus end). The Monte Carlo J_1 value can presumably be raised, while keeping c_o constant, by increasing α_{1T} and decreasing α_{1D} (c_o is very sensitive to α_{1D}). But this possibility has not been explored.

Results for microtubules on nucleated sites

Here we use the four macroscopic rate constant curves (J_1, J_2, k, k') in Figs. 3 and 4 to calculate steady-state properties of MTs attached to nucleated sites (3) (each MT has one free end). The kinetic two-phase model is shown in Fig. 5 (this is the same as figure 6 in ref. 8). Some of the steady-state properties of the model, derived and discussed in ref. 8, are

$$x = J_1(k' - J_2)/-J_2(k + J_1) \cong J_1/(k + J_1) \quad [6]$$

$$P_0 + f_1 + f_2 = 1 \quad [7]$$

$$P_0 = -J_2(1 - x)/(J_1 - J_2) \quad [8]$$

Table 1. Monte Carlo results at $c = 10$

Transition	Time, s	p_1	p_2	p_3	p_4	p_5	J, s^{-1}
57,200	6.7992	2.8197	4.9895	4.9889	4.9898	5.0000	5.801
57,400	8.7035	2.2567	4.9924	4.9964	4.9927	4.9699	3.714
57,600	16.804	1.7864	2.2369	1.8337	1.5542	1.4213	−1.575
57,800	0.38280	0.0000	0.0000	0.0000	0.0000	0.0000	−520.6
58,000	0.36938	0.0000	0.0000	0.0000	0.0000	0.0000	−539.5
58,200	0.38872	0.0000	0.0000	0.0000	0.0000	0.0000	−512.6
58,400	0.35918	0.0000	0.0000	0.0000	0.0000	0.0000	−554.8
58,600	1.3256	0.7530	0.3211	0.0000	0.0000	0.0000	−148.3
58,800	0.37413	0.0000	0.0000	0.0000	0.0000	0.0000	−532.6
59,000	3.2877	1.6185	0.0000	0.0000	0.0000	0.0000	−57.90
59,200	0.38220	0.0000	0.0000	0.0000	0.0000	0.0000	−521.4
59,400	7.5177	2.1469	2.2735	2.2186	2.0271	1.8015	4.418
59,600	10.597	2.4359	4.9967	4.9968	4.9894	4.9910	4.506
59,800	10.978	2.3389	4.6705	4.3159	4.0591	3.7912	3.019
60,000	11.695	2.3073	3.7638	3.5925	3.4479	3.3429	6.812
60,200	14.391	2.2966	3.6267	3.3407	2.8837	2.5589	3.092
60,400	4.8353	3.6770	4.9780	4.9727	4.6107	4.5887	25.85
60,600	3.0871	4.3545	4.9777	4.9611	4.9518	4.9690	45.95
60,800	5.8251	2.8875	5.0000	5.0000	5.0000	5.0000	16.39
61,000	5.0592	2.9907	5.0000	5.0000	5.0000	5.0000	22.86

Table 2. Monte Carlo snapshots at $c = 10$

Transition	Surface structure	Ts in helices	Deepest Ts
49,000	0,1,3,0,9	0,0,0,0,0	0,0,0,0,0
50,000	6,1,1,0,5	0,0,0,0,0	0,0,0,0,0
51,000	0,1,0,11,1	19,16,14,9,15	19,16,14,9,18
52,000	0,2,5,0,6	27,29,54,52,32	37,51,54,59,49
53,000	6,1,1,3,2	106,112,104,109,98	106,112,109,109,110
54,000	7,2,1,2,1	69,77,67,72,69	89,96,97,96,90
55,000	7,6,0,0,0	63,67,68,64,59	70,86,93,91,70
56,000	1,1,8,0,3	118,112,96,111,110	128,128,123,126,125
57,000	0,0,0,13,0	47,33,27,28,50	104,84,27,29,102
58,000	6,3,2,1,1	0,0,0,0,0	0,0,0,0,0
59,000	2,3,0,3,5	0,0,0,0,0	0,0,0,0,0
60,000	2,0,0,0,11	13,7,7,7,3	13,7,7,7,4
61,000	0,0,0,3,10	83,87,75,67,76	87,87,87,81,77

$$f_1 = P_0\, x/(1 - x) \quad [9]$$

$$\overline{m} = 1/(1 - x) \quad [10]$$

$$P_{occ} = (J_1 - J_2 x)x^{m_0}/(J_1 - J_2) \cong x^{m_0+1}. \quad [11]$$

The approximation in Eq. **6** is accurate for the smaller c values. Note that $x \cong 1/2$ when $J_1 = k$, and $x = 0$ when $J_1 = 0$. The f_1 for an attached polymer (Eq. **9**) differs considerably from the f_1 in Eq. **4** and Fig. 4 for one end of a very long MT in solution. However, the two f_1s have the same value (0.865 in this example) at $c = c_o$, where $x = 1$. The quantity $\overline{m}$ is the mean size of MTs with $m \geq 1$ and P_{occ} is the probability that $m > m_0$ (the size needed for detection). Calculated curves of x, f_1 (attached), P_{occ} (solid curve; using $m_0 = 500$), and $\overline{m}$, as functions of c, are shown in Fig. 6. We use a five times larger m_0 here than in ref. 8 because there are five helices (this m_0 corresponds to a length of 0.3 μm). Compared with the corresponding curves in figure 2 of ref. 8, we observe here that x is near 1 even for quite small c/c_o (because J_1 is much larger). Consequently, P_{occ} starts its upward trend at a much smaller c/c_o, despite the larger m_0. The experimental curve (figure 4 of ref. 3) starts up at about $c/c_o = 0.2$. Correspondingly, $\overline{m}$ also reaches large values at relatively small c/c_o. It should be noted that the x curve must drop quite sharply for $c < 2$ because $x \cong 1/2$ at $J_1 = k$ and $x = 0$ at $J_1 = 0$.

Inspection of this Monte Carlo example shows that it is a quite good approximation to use

$$P_{occ} \cong \left(\frac{J_1}{k + J_1}\right)^{m_0+1} \quad [12]$$

Table 3. Some properties at several values of c

c	J_h, s^{-1}	$\overline{N}$	No. of phase changes
0	0.384	0	0
1.5	0.556	0.125	0
3	0.978	1.07	2
4.5	1.98	6.89	8
6	6.70	69.2	23
7	9.75	111	50
8	10.8	129	54
9	13.2	172	54
10	14.7	198	59
11	15.9	214	62
13	18.6	258	48
15	20.0	286	25

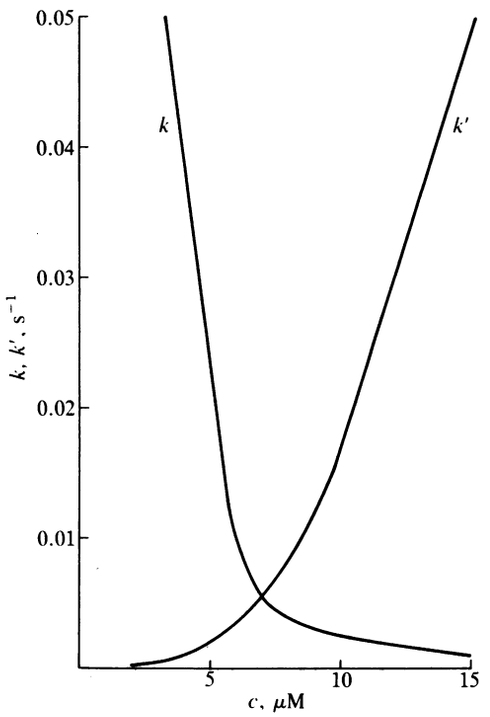

FIG. 3. Phase-change constants k and k', as functions of c, found in the Monte Carlo example used.

up to about $c/c_o = 0.7$. We have already noted that the experimental J_1 line (for the plus end) is significantly above the Monte Carlo J_1 curve. If we make a hybrid calculation using the Monte Carlo k from Fig. 3 and the larger experimental J_1 (this is $5.364c - 0.37$, with the c scale adjusted to our c_o value), Eq. **12** leads to the dashed curve in Fig. 6 for P_{occ}. This curve starts up at about $c/c_o = 0.2$, in agreement with experiment (3).

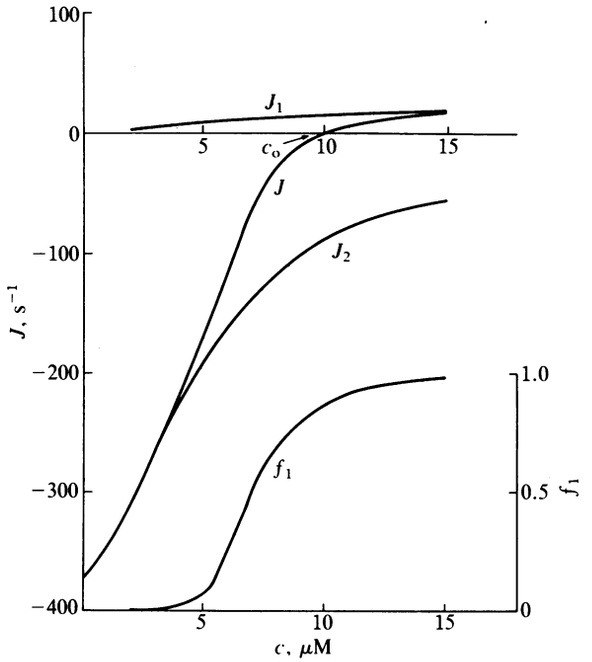

FIG. 4. Macroscopic rate constants J_1 and J_2 (mean growth rate in the two phases) found in the Monte Carlo example. J is the composite growth rate of the MT end at steady state, from Eq. **5**. The critical concentration is $c_o = 9.97$ (the value of c at which $J = 0$). The f_1 curve represents the fraction of time the MT end is in state 1 (growing, with cap), at steady state. At $c = c_o$, $f_1 = 0.865$.

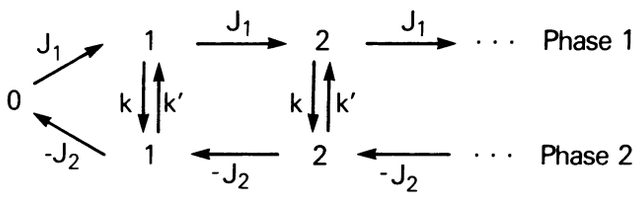

FIG. 5. Kinetic scheme for a two-phase MT aggregating on a nucleated site. The integers 0, 1, 2, ... are values of m, the number of subunits in the aggregate. The probability of state 0 (empty site) is P_0.

Going one step further, one could use experimental curves for $P_{occ}(c)$ and $J_1(c)$ in Eq. **12** to deduce $k(c)$—a quantity not easy to measure directly. The Mitchison–Kirschner curve

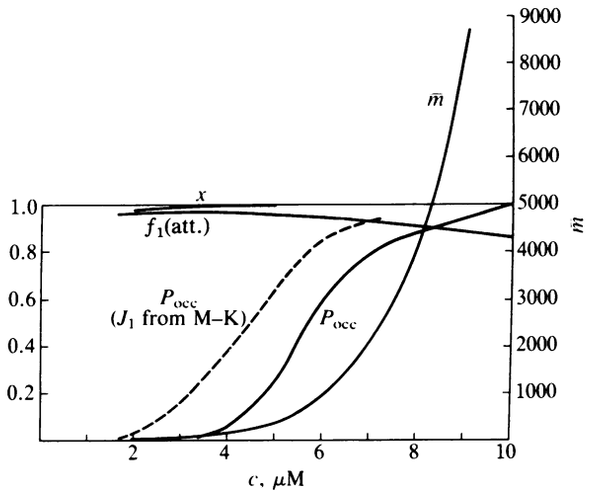

FIG. 6. Plots of x, f_1, $\bar{m}$, and P_{occ} (solid curves) from Eqs. **6, 9, 10**, and **11**, using the Monte Carlo rate constant functions k, k', J_1, and J_2 in Figs. 3 and 4 and $m_0 = 500$. The dashed curve for P_{occ} is based on Eq. **12**, using the Mitchison–Kirschner (M–K, ref. 4) J_1 line.

Table 4. Calculation of k from experimental data

c, μM	P_{occ}	J_1, s^{-1}	k, s^{-1}
5	0.138	18.73	0.0742
7.5	0.315	28.28	0.0653
10	0.512	37.83	0.0506

For experimental data, see refs. 3 and 4.

for P_{occ} (figure 4 of ref. 3) cannot be a true steady-state curve because P_{occ} does not reach saturation at $c = 14$ (the operational c_0). However, if we ignore this for purposes of illustration and use $J_1 = 3.82c - 0.37$ (table 1 of ref. 4, with the Mitchison–Kirschner c scale), we can use Eq. **12** (with $m_0 = 500$) to find the k values in Table 4. These are somewhat larger than k in Fig. 3.

In summary, the two-phase model, using macroscopic rate constants derived from Monte Carlo analysis of a microscopic five-start helix model for a MT, appears to be consistent, semiquantitatively, with the steady-state experimental results of Mitchison and Kirschner (3, 4). A closer fit was not attempted because of computer expense.

1. Hill, T. L. & Chen, Y. (1984) *Proc. Natl. Acad. Sci. USA* **81,** 5772–5776.
2. Carlier, M. F., Hill, T. L. & Chen, Y. (1984) *Proc. Natl. Acad. Sci. USA* **81,** 771–775.
3. Mitchison, T. & Kirschner, M. W. (1984) *Nature (London)* **312,** 232–237.
4. Mitchison, T. & Kirschner, M. W. (1984) *Nature (London)* **312,** 237–242.
5. Hill, T. L. & Kirschner, M. W. (1982) *Int. Rev. Cytol.* **78,** 1–125.
6. Hill, T. L. & Carlier, M. F. (1983) *Proc. Natl. Acad. Sci. USA* **80,** 7234–7238.
7. Carlier, M. F. & Pantaloni, D. (1982) *Biochemistry* **21,** 1215–1224.
8. Hill, T. L. (1984) *Proc. Natl. Acad. Sci. USA* **81,** 6728–6732.
9. Chen, Y. & Hill, T. L. (1983) *Proc. Natl. Acad. Sci. USA* **80,** 7520–7523.